

CVM-Cervix: A Hybrid Cervical Pap-Smear Image Classification Framework Using CNN, Visual Transformer and Multilayer Perceptron

Wanli Liu^a, Chen Li^{a,*}, Ning Xu^b, Tao Jiang^c, Md Mamunur Rahaman^a, Hongzan Sun^d, Xiangchen Wu^e, Weiming Hu^a, Haoyuan Chen^a, Changhao Sun^{a,f}, Yudong Yao^g, Marcin Grzegorzek^h

^a*Microscopic Image and Medical Image Analysis Group, College of Medicine and Biological Information Engineering, Northeastern University, Shenyang, China*

^b*Liaoning Petrochemical University, Fushun, China*

^c*School of Control Engineering, Chengdu University of Information Technology, Chengdu, China*

^d*Shengjing Hospital, China Medical University, Shenyang, China*

^e*Suzhou Ruiqian Technology Company Ltd., Suzhou, China*

^f*Shenyang Institute of Automation, Chinese Academy of Sciences, Shenyang, China*

^g*Department of Electrical and Computer Engineering, Stevens Institute of Technology, Hoboken, US*

^h*Institute of Medical Informatics, University of Luebeck, Luebeck, Germany*

Abstract

Cervical cancer is the seventh most common cancer among all the cancers worldwide and the fourth most common cancer among women. Cervical cytopathology image classification is an important method to diagnose cervical cancer. Manual screening of cytopathology images is time-consuming and error-prone. The emergence of the automatic computer-aided diagnosis system solves this problem. This paper proposes a framework called CVM-Cervix based on deep learning to perform cervical cell classification tasks. It can analyze pap slides quickly and accurately. CVM-Cervix first proposes a

*Corresponding author

Email address: lichen201096@hotmail.com (Chen Li)

Convolutional Neural Network module and a Visual Transformer module for local and global feature extraction respectively, then a Multilayer Perceptron module is designed to fuse the local and global features for the final classification. Experimental results show the effectiveness and potential of the proposed CVM-Cervix in the field of cervical Pap smear image classification. In addition, according to the practical needs of clinical work, we perform a lightweight post-processing to compress the model.

Keywords: Convolutional Neural Network, Visual Transformer, Multilayer Perceptron, Cervical cancer, Pap smear, Image classification

1. Introduction

Cervical cancer is the seventh most common cancer among all the cancers worldwide and the fourth most common cancer among women. In underdeveloped countries, the mortality rate from cervical cancer is very high. Premature sexual intercourse, intercourse with multiple partners, early pregnancy, weak immune system, smoking, having oral contraceptives, and improper menstrual hygiene are the leading causes of cervical cancer. The common symptoms of cervical cancer are abnormal vaginal bleeding, vaginal discharge, and moderate pain during sexual intercourse [1]. If it can be detected early and given the proper treatment, cervical cancer can be prevented.

Cytopathology screening is widely practised to diagnose cervical malignancies. The procedure of cervical cytopathological examination is that a doctor collects cells on a patient's cervix using brushes and then places the exfoliated cells on a glass slide. Cytopathologists observe under the micro-

scope to determine whether there is a malignant tumor. However, there are thousands of cells on each slide [2]. Therefore, manual inspection is very troublesome, and experts are prone to make mistakes. So this problem needs a better solution.

The emergence of the automatic computer-aided diagnosis system (CAD) solves this problem. CAD can analyze pap slides quickly and accurately. Early CAD was based on classical image processing and traditional machine learning methods, where the manually designed features may lead to unsatisfactory classification results [3]. Nowadays, deep learning technology is relatively mature, and it makes achievements in computer vision, medical imaging, Natural Language Processing (NLP), and other fields. Deep learning technology is different from classical machine learning, and it can automatically learn features for classification [4]. However, training a deep learning model requires a large number of labelled data sets.

Convolutional Neural Network (CNN) is currently a popular deep learning network, widely used in image segmentation, detection and classification [5, 6, 7]. Recently, Visual Transformer (VT), which originally uses Transformer to process NLP tasks, appears in the field of computer vision. The VT model that first appeared in the field of computer vision is Vision Transformer (ViT). On the premise of pre-training with a large amount of data, it is better than the latest convolutional network, and the computing resources required for training are greatly reduced [8].

In this study, we introduce CVM-Cervix that uses CNN, VT and Multi-layer Perceptron (MLP). We have combined SIPaKMeD and CRIC datasets, consisting of 11 categories of single-cell cervical cytopathological images [9,

10]. CVM-Cervix achieves a classification accuracy of 91.72%. The workflow of CVM-Cervix is shown in Fig. 1. From the workflow diagram, it can be seen that:

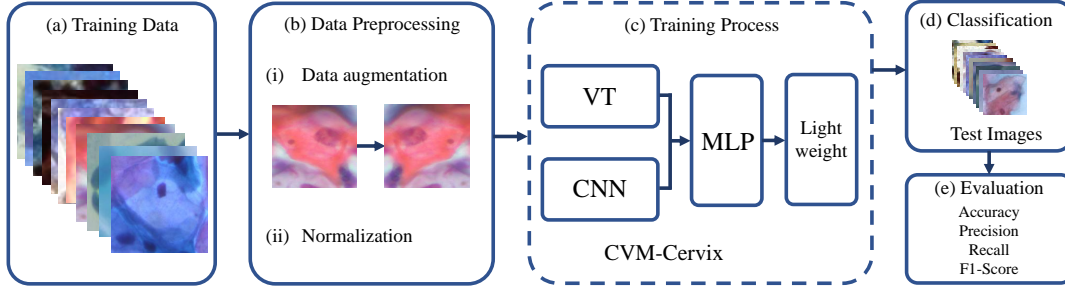


Figure 1: Workflow of the proposed CVM-Cervix model.

- (a) Cervical cytopathological images are obtained from SIPaKMeD and CRIC datasets and used as the training data. Sec. 4 explains the details of the dataset.
- (b) In the preprocessing stage, the training datasets are augmented and normalized.
- (c) In this stage, the preprocessed data are fed into CNN and VT modules to extract local and global features. Then, the extracted features are input into MLP module for fusion and classification. Furthermore, we introduce a lightweight post-processing to compress the model.
- (d) In this stage, unseen test images are supplied to CVM-Cervix for classification.
- (e) Finally, the performance of CVM-Cervix is evaluated by calculating the precision, recall, F1-Score, and accuracy.

The main contributions of this paper are as follows: (1) This study performs a 11-class classification task, and it is the work with the most complex data and the most types in the existing literature. (2) A new method (CVM-Cervix) is proposed, which uses CNN, VT and MLP modules for feature extraction and fusion to improve the overall classification performance. In addition, a lightweight post-processing is used to compress the model. (3) The performance of our CVM-Cervix exceeds that of existing methods and achieves a good result of 91.72%.

This paper structure is as follows: Sec. 2 elaborates the application and related methods of deep learning in cervical cell image classification tasks. Sec. 3 describes our proposed CVM-Cervix. Sec. 4 explains the dataset, experimental results, experimental environment, and evaluation methods. Sec. 5 discusses some issues in our proposed CVM-Cervix. Sec. 6 summarizes this paper and proposes future work directions.

2. Related work

2.1. Deep neural networks

This subsection provides a brief introduction to some common deep neural networks.

There are many classic CNN models. Xception network introduces depth-wise separable convolutions, which improves efficiency. This method separates spatial convolution and channel convolution [11]. VGG network uses deeper networks and smaller filters. This work uses a 3×3 filter, which has the same acceptance field as a 7×7 filter, but the amount of parameters is greatly reduced [12]. ResNet network introduces residual blocks. The

residual network can turn the deep network into a shallow network by setting other layers in the deep network as identity mapping [13]. DenseNet network introduces direct connections between any two layers with the same feature map size. DenseNet can be extended to hundreds of layers and still be optimized [14]. In [15], an end-to-end attentional recurrent convolutional network is proposed. The method can learn to focus on some important locations and process them on high-level features, discarding unimportant information to improve classification accuracy. In [16], a multi-scale scene classification method based on a two-stream architecture is proposed. Global and local streams of this method can extract global and local features of the image, respectively. This method proposes a key region detection strategy to connect global and local streams.

Many Visual Transformer models appear. ViT model applies Transformer in the field of NLP to the field of computer vision. Under the training of a large amount of data, the effect of ViT is better than CNN [8]. BoTNet combines self-attention and ResNet. While obtaining local information, it also can obtain global information. While reducing the number of parameters, the effect is better than ResNet [17]. DeiT introduces distillation tokens, which are added after the image block sequence. The training of DeiT requires fewer data and fewer computing resources [18]. T2T-ViT proposes a new T2T mechanism based on ViT, which overcomes the shortcomings of the original simple tokenization. T2T-ViT requires fewer parameters than ViT, but the effect is better [19].

2.2. Applications of deep learning in cervical cell image classification tasks

This subsection introduces applications of deep learning in cervical cytopathology image classification. Please follow our review paper about cervical cytopathology image analysis using deep learning for further information [20].

In [21], the performances of the ResNet and VGG networks are evaluated. For the cervical dataset, the accuracy rate varies between 84-86%. The results show that ResNet has higher accuracy and smaller standard deviation, which is a better network. In [22], a hybrid deep feature fusion method based on deep learning is proposed. This method uses pre-trained VGG16, VGG19, Xception, and ResNet50 to extract features and uses a feature fusion technology. This method achieves an accuracy of 99.85% for a binary classification task of the SIPaKMeD dataset. A method for cervical cell classification based on graph convolutional network (GCN) is proposed [23]. This method uses the CNN features of the image for clustering and then constructs the graph structure. GCN can generate relationship-aware features, which are merged into CNN features to enhance feature expressiveness. This method has an accuracy of 98.37% for a 5-class task.

As can be seen from the references, most studies use the CNN model for classification or feature extraction. None of the studies uses CNN and VT models for cervical cell classification tasks. The CNN model can only extract the local features of the image through the convolution kernel, and the VT model can extract the global features of the image through the attention mechanism. We combine local and global features of the image for better analysis. Therefore, this research is noble and significant in this field.

3. Method

3.1. CVM-Cervix

The CVM-Cervix framework is designed to classify cervical cell images and Fig. 2 is a structural diagram of CVM-Cervix:

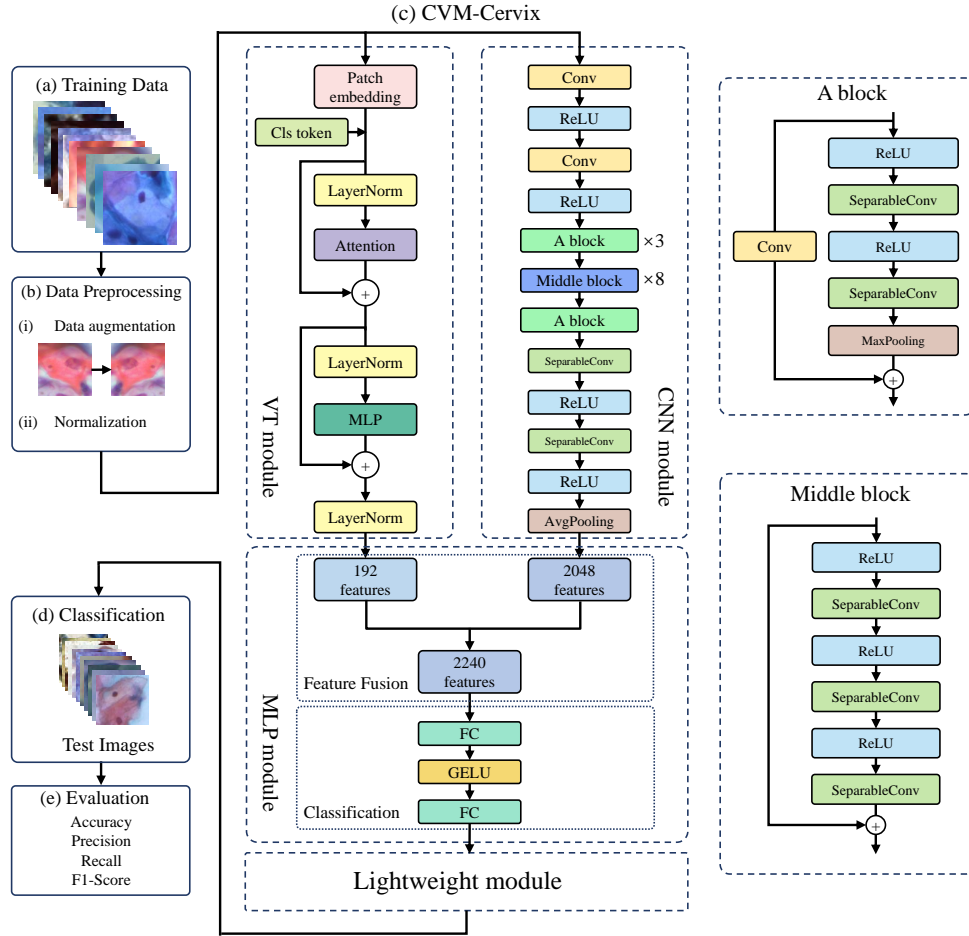


Figure 2: The structure of CVM-Cervix.

- Fig. 2 (a) shows the cervical cell images used to train CVM-Cervix.

- Fig. 2 (b) demonstrates the data preprocessing stage. In the preprocessing stage, the first step is data augmentation: first, the input images are resized to 224×224 pixels. Then the random horizontal flip function is used, and the image has a 50% probability of being flipped horizontally, which can enhance the generalization ability of CVM-Cervix. The second step is to normalize the training data. The training data are input into CVM-Cervix after the preprocessing stage.
- Fig. 2 (c) shows the main body of CVM-Cervix, which consists of three parts. First, CVM-Cervix designs VT and CNN modules for global and local feature extraction. Then, a MLP module is introduced for feature fusion and classification [11, 18]. In VT module, we use a tiny DeiT model without distillation tokens, which is equivalent to the ViT model with improved parameters. This module retains all the structure of the DeiT model except the final classification layer, and finally, 192 features are extracted. CNN module uses the official model of Xception, and also retains all the structure except the final classification layer. CNN module finally extracts 2048 features. In MLP module, the 192 and 2048 features extracted by VT and CNN modules are first fused to generate 2240 features. Then, MLP is used for classification. MLP consists of two fully connected layers containing the GELU activation function. Furthermore, we post-process the model using a lightweight module to achieve compression.
- In Fig. 2 (d), we use CVM-Cervix to classify the invisible test images.
- In Fig. 2 (e), the performance of CVM-Cervix is evaluated by calculat-

ing precision, recall, F1-Score, and accuracy.

3.2. CNN module for local feature extraction

In CVM-Cervix, CNN module is designed to extract local features of cervical cell images. We use the structure other than the fully connected layer in the Xception model as CNN module to extract 2048-dimensional features. The basic components of CNN module are the convolutional layer and the pooling layer. The convolutional layer extracts image features through the function of the convolution kernel. There are two types of pooling layers: the maximum pooling layer and the average pooling layer, which reduce the number of features by looking for the maximum or average value. The advantage of this CNN module is the use of depthwise separable convolution, which is a combination of depthwise convolution and pointwise convolution. Fig. 3 shows the structure of depthwise separable convolution. Depthwise separable convolution has a lower parameter number and operation cost compared with the conventional convolution operation.

3.3. VT module for global feature extraction

In CVM-Cervix, VT module is introduced for global feature extraction in cervical cell images. We use the tiny DeiT model without distillation token as VT module to extract 192-dimensional features. The tiny DeiT model without distillation token is equivalent to the ViT model with improved parameters. VT module converts the image into a patch sequence to process 2D images. Then, the patch sequence is flattened and mapped to the required dimension by linear projection. In addition, positional information and classification headers are added to facilitate learning. This sequence is input

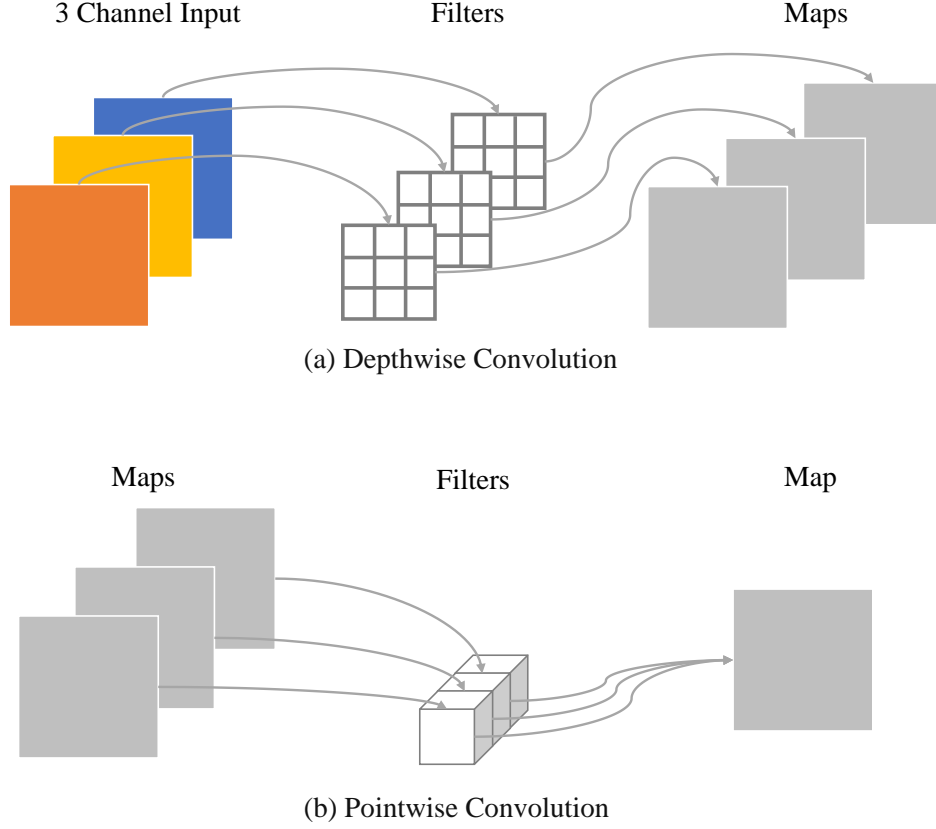


Figure 3: The structure of depthwise separable convolution.

into the Transformer encoder. The Transformer encoder contains multi-head self-attention and MLP blocks. There is a LayerNorm before each block, and residual connection is applied after each block.

3.4. MLP module for feature fusion and classification

In CVM-Cervix, MLP module is used for feature fusion and classification, where an early fusion strategy is applied. The traditional methods of early fusion include serial and parallel fusion. We chose the serial fusion method. If the dimensions of the two input features are m and n , then the dimension

of the output feature is $m + n$. Therefore, the fusion process is to concatenate the 2048-dimensional features extracted by CNN module and the 192-dimensional features extracted by VT module to obtain 2240-dimensional features.

Furthermore, a MLP classifier is designed for the final classification. MLP is the most brief and effective artificial neural network algorithm, and it is a feedforward neural network. It learns through backpropagation technology. MLP has an input layer, a hidden layer, and an output layer. The input layer is the receiver of MLP. There can be one or more hidden layers in the middle, which are used to calculate data and iterate. The output layer can predict the classification result. The simplest MLP contains only one hidden layer, which is a three-layer structure. The use of the activation function can introduce nonlinearity to the neural network and enhance the expressive ability of the network. The MLP here is two fully connected layers containing GELU activation functions, which are used to classify 2240-dimensional features.

4. Experiments and analysis

4.1. Datasets

4.1.1. CRIC

The CRIC dataset has 400 images from traditional Pap smears, including 11534 cells manually classified [10]. It is classified by several cytopathologists according to the Bethesda system nomenclature. There are six types of images: atypical squamous cells, cannot exclude a high-grade lesion (ASC-H); atypical squamous cells of undetermined significance, possibly non-neoplastic (ASC-US); squamous cell carcinoma (SCC); high-grade squamous intraepi-

ithelial lesion (HSIL); low-grade squamous intraepithelial lesion (LSIL); negative for intraepithelial lesion or malignancy (NILM) [10]. In this paper, only cropped images are used, including 4789 images of separated cervical cells [24]. Some examples can be seen in Fig. 4.

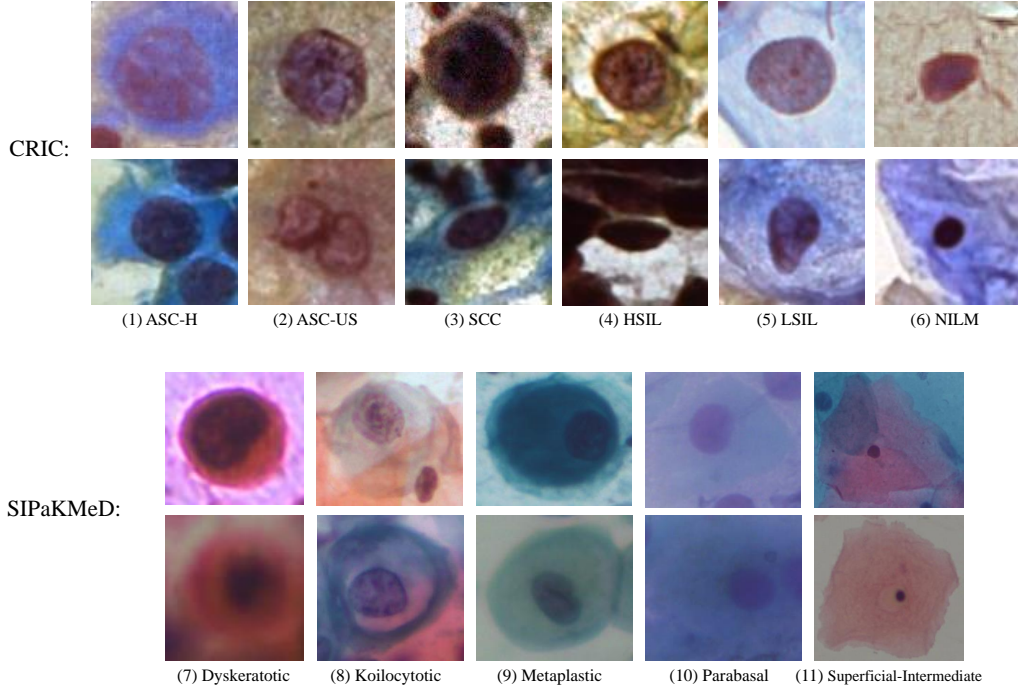


Figure 4: An example of images in CRIC and SIPaKMeD datasets.

4.1.2. *SIPaKMeD*

The SIPaKMeD dataset can be used for cervical cell image classification tasks. This dataset contains 4049 cervical cell images cropped from the clustered cell images, which are obtained by the CCD camera. There are five categories of these images: dyskeratotic, koilocytotic, metaplastic, parabasal, and superficial intermediate [9]. Fig. 4 shows some examples.

4.1.3. Combined dataset

In this study, we have combined the CRIC and SIPaKMeD datasets and used them in this experiment. Therefore, we obtained 11 categories, including six categories of the CRIC dataset and five categories of the SIPaKMeD dataset. This combined dataset has a total of 8838 images. We randomly selected 60% of the images in each class to serve as the training set, 20% as the validation set, and 20% as the test set. The data settings are shown in Table 1.

Table 1: Data settings of the combined dataset.

Class/Dataset	Train	Validation	Test	Total
(1) ASC-H	484	161	161	806
(2) ASC-US	446	148	148	742
(3) SCC	413	137	137	687
(4) HSIL	525	175	174	874
(5) LSIL	491	164	163	818
(6) NILM	518	172	172	862
(7) Dyskeratotic	488	163	162	813
(8) Koilocytotic	495	165	165	825
(9) Metaplastic	476	159	158	793
(10) Parabasal	473	157	157	787
(11) Superficial-Intermediate	499	166	166	831
Total	5308	1767	1763	8838

4.2. Experimental environment

The experiments in this paper are carried out on a local workstation with 32GB RAM and the windows 10 operating system. The GPU of the workstation is an 8GB NVIDIA Quadro RTX 4000. We use the Python programming language, and the version of Pytorch is 1.8.0. When training CVM-Cervix, the learning rate is set to 0.0002, the batch size of the training set is 16, the epoch is 100, and the AdamW optimizer is used.

4.3. Evaluation methods

Precision, recall, F1-Score, and accuracy are calculated to evaluate the performance of CVM-Cervix. True Positive (TP) is the number of positive samples predicted accurately. True Negative (TN) is the number of negative samples predicted accurately. The number of negative samples predicted to be positive is False Positive (FP). And the number of positive samples predicted to be negative is False Negative (FN). The proportion of TP in all positive predictions is precision. A recall is the ratio of predicted positive samples to the total positive sample numbers. F1-Score is a comprehensive indicator of precision and recall. Accuracy is the ratio of the number of correct predictions to the total. The formulas are shown in Table 2.

4.4. Experimental results and analysis

In the validation and test phases, the precision, recall, F1-Score, and accuracy are calculated to evaluate the performance of the proposed CVM-Cervix model, as shown in Fig. 5. It can be seen that the precision, recall, F1-Score, and accuracy of CVM-Cervix on the validation set are 92.80%, 92.90%, 92.80%, and 92.87%, respectively. The precision, recall, F1-Score,

Table 2: Evaluation metrics

Assessment	Formula	Assessment	Formula
Precision (P)	$\frac{TP}{TP+FP}$	F1-Score	$2 \times \frac{P \times R}{P+R}$
Recall (R)	$\frac{TP}{TP+FN}$	Accuracy	$\frac{TP+TN}{TP+TN+FP+FN}$

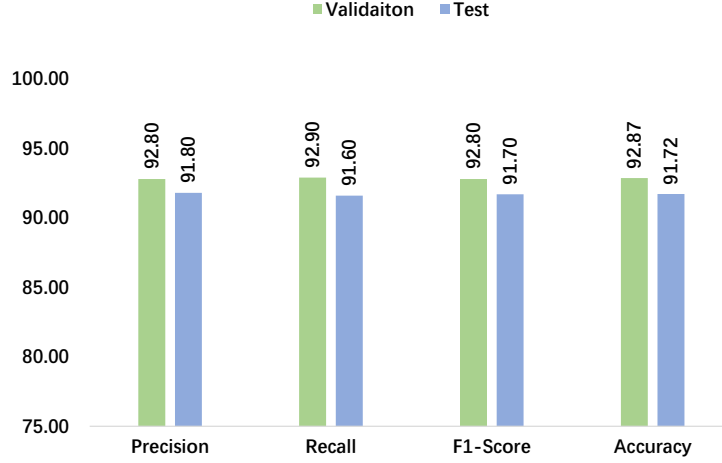


Figure 5: The performance of CVM-Cervix.

and accuracy of CVM-Cervix on the test set are 91.80%, 91.60%, 91.70%, and 91.72%, respectively. The performance difference of CVM-Cervix on the validation set and the test set is about 1%, which proves its strong generalization ability. The performance of CVM-Cervix surpasses the existing methods and achieves very good results.

The confusion matrices of the validation and test results using CVM-Cervix are shown in Fig. 6. In the validation confusion matrix, we can see that the classifications of the first, the third, and the sixth to the eleventh

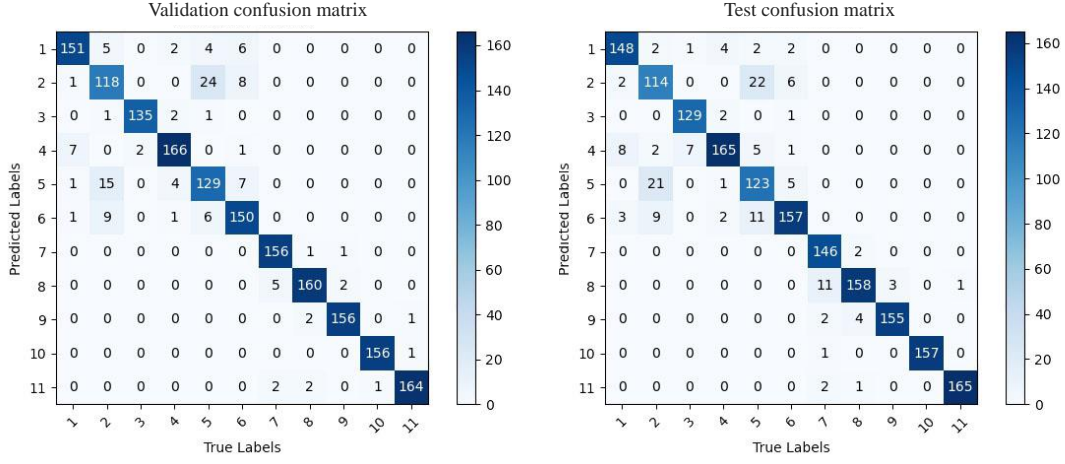


Figure 6: The confusion matrices of the validation and test results using CVM-Cervix.

categories are very accurate. Fifteen images of the second category are classified into the fifth category, and nine images are classified into the sixth category. Twenty-four images of the fifth category are classified into the second category. The situation is roughly the same on the test confusion matrix. Twenty-one images of the second category are misclassified into the fifth category, and nine images are misclassified into the sixth category. Twenty-two images of the fifth category are misclassified into the second category, and 11 images are misclassified into the sixth category. In the seventh category, 11 images are misclassified into the eighth category.

Among these eleven categories, the first, third, fourth, seventh, and eighth types are abnormal types. It can be observed that CVM-Cervix has a higher classification accuracy for abnormal types. We hope that the model will not misclassify cancer patients in practical applications, because this is a matter of life and death. Therefore, the higher the accuracy of the model's classification of abnormal types, the better, which is exactly the performance

of our CVM-Cervix.

4.5. Computational time

In this experiment, we use 100 epochs to train CVM-Cervix, and the model parameter size is about 120 MB. There are 5308 training images, and the total training time is 2.3 hours. The training time for each epoch is about 82 seconds. Although the training time is long, the test time is only 31 seconds. There are 1763 test images, and the test time for each image is about 0.018 seconds.

4.6. Lightweight post-processing

In addition, according to the practical needs of clinical work, we perform a lightweight post-processing to compress the model [25]. Firstly, we use a quantization technique to reduce the number of bits required to store each weight from 32 to 16 bits. Then, the model parameter size is reduced to 60 MB. Finally, the classification performance is almost unchanged (around -1%), and the total training time is shortened (around 1 hour).

4.7. Extended experiment

4.7.1. Extended experiment on the Combined dataset: comparative experiment

To see the performance of CVM-Cervix, 22 models are selected for this comparative experiments, including 18 CNN models: VGG11 [12], VGG13 [12], VGG16 [12], VGG19 [12], ResNet18 [13], ResNet34 [13], ResNet50 [13], ResNet101 [13], DenseNet121 [14], DenseNet169 [14], InceptionV3 [26], Xception [11], AlexNet [27], GoogLeNet [28], MobileNetV2 [29], ShuffleNetV2 \times 1.0 [30],

ShuffleNetV2 \times 0.5 [30], InceptionResNetV1 [31]. The remaining four are VT models: ViT [8], BoTNet [17], DeiT [18], T2T-ViT [19].

The experimental settings are the same. Table 3 shows the results of models on the test set of the combined dataset. It can be seen that DenseNet169 obtains the highest accuracy rate of 88.99% in CNN models. In VT models, DeiT has the highest accuracy rate of 87.35%. Among all the models, the proposed CVM-Cervix achieves the highest test accuracy of 91.72%, which is nearly 3% higher than the accuracy of DenseNet169 and DeiT. In addition, the precision, recall, and F1-Score of CVM-Cervix are also the highest, which are 91.80%, 91.60%, and 91.70%, respectively. This shows the effectiveness of the proposed CVM-Cervix model.

4.7.2. Extended experiment on Combined dataset: classification with data augmentation

In this extended experiment, the training set is augmented. The data increase four times by rotating 180 degrees, flipping left and right, and flipping up and down. Then CVM-Cervix is used on the augmented training set for the experiment. The comparison of test results of CVM-Cervix on the unaugmented and augmented training sets are shown in Fig. 7.

It can be seen that the precision, recall, F1-Score, and accuracy of CVM-Cervix on the augmented training set are 93.60%, 93.50%, 93.50%, and 93.48%, respectively. There is a roughly 2% improvement compared to the effect on the unaugmented training set. The reason for the improvement is the increase in data so that CVM-Cervix can be better trained. The improvement is not large because the performance of the proposed CVM-Cervix model on the unaugmented training set has stabilized. It also illustrates the

Table 3: Comparison results of models on the test set of the combined dataset.

Models	Avg. P	Avg. R	Avg. F1	Acc (%)
VGG11	84.80	83.90	84.00	84.06
VGG13	85.30	84.70	84.40	84.62
VGG16	79.80	79.90	79.60	79.97
VGG19	78.60	78.30	78.20	78.38
ResNet18	88.40	88.30	88.20	88.25
ResNet34	88.00	88.10	87.90	88.03
ResNet50	87.60	87.60	87.30	87.57
ResNet101	86.50	86.40	86.30	86.38
DenseNet121	87.90	87.80	87.70	87.86
DenseNet169	89.20	88.90	88.70	88.99
InceptionV3	85.40	84.90	84.80	84.96
Xception	87.70	87.70	87.60	87.69
AlexNet	86.20	86.20	86.10	86.10
GoogLeNet	87.60	87.20	87.10	87.29
MobileNetV2	84.90	84.60	84.60	84.62
ShuffleNetV2 \times 1.0	85.50	84.30	84.50	84.57
ShuffleNetV2 \times 0.5	82.60	82.60	82.50	82.64
InceptionResNetV1	85.20	84.90	84.90	84.96
ViT	86.10	86.00	85.70	85.87
BoTNet	66.10	65.50	63.90	65.51
DeiT	87.40	87.40	87.20	87.35
T2T-ViT	85.60	85.30	85.20	85.19
CVM-Cervix	91.80	91.60	91.70	91.72

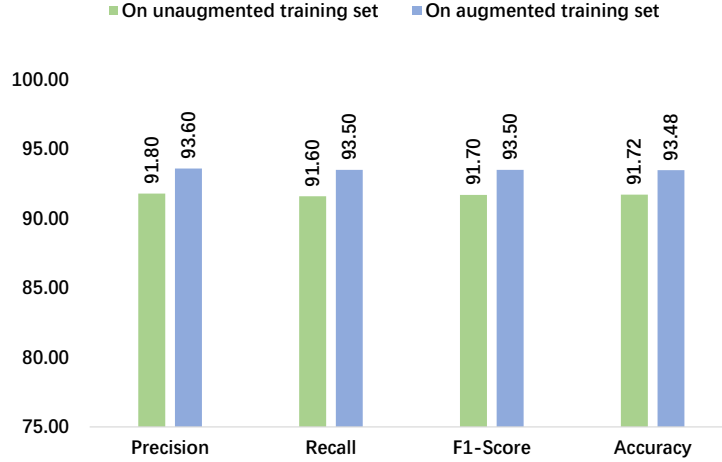


Figure 7: The comparison of test results of CVM-Cervix on the unaugmented and augmented training sets.

superiority of our CVM-Cervix.

4.7.3. Extended experiment on Herlev dataset

To validate the generalization ability of CVM-Cervix on other cervical Pap smear datasets, we use Herlev dataset for extended experiments [32]. The experimental setup is the same as the main experiment. There are two types in the Herlev dataset: Normal and Abnormal. Some examples are shown in Fig. 8. This dataset has 917 images, and we randomly divide the training set, validation set and test set in a ratio of 6:2:2. Due to the small amount of data, we augment the training set 4 times. The data settings are shown in Table 4.

Fig. 9 shows the performance of CVM-Cervix on the Herlev dataset. It can be seen that the precision, recall, F1-Score and accuracy on the validation set are 96.40%, 95.10%, 95.80% and 96.72%, respectively. The precision, recall, F1-Score and accuracy on the test set are 88.90%, 93.50%, 90.70%

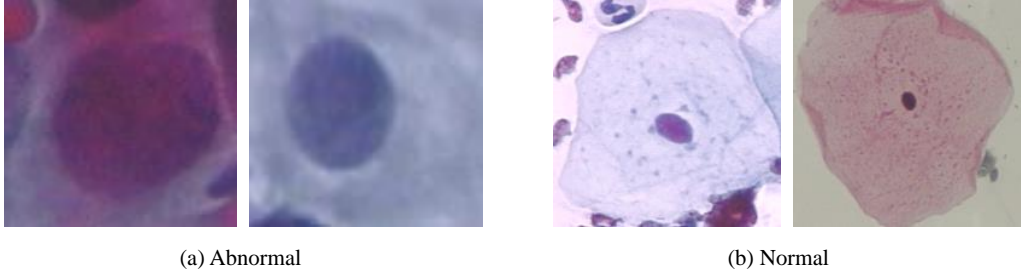


Figure 8: An example of images in Herlev dataset.

Table 4: Data settings of the Herlev dataset.

Class/Dataset	Train	Validation	Test	Total
Abnormal	1620	135	135	1890
Normal	584	48	48	680
Total	2204	183	183	2570

and 92.35%, respectively. CVM-Cervix performs slightly less well on the test set due to too little data and an uneven number of classes, but still good. It indicates that CVM-Cervix generalizes well on other cervical Pap smear datasets.

4.7.4. Extended experiment on peripheral blood cell dataset

To explore the performance of CVM-Cervix on other cell image datasets, the peripheral blood cell dataset is used for extended experiments [33]. There are 17092 blood cell images in this dataset, with eight types: neutrophil, eosinophil, basophil, lymphocyte, monocyte, immature granulocyte, erythroblast and platelet. Some examples are shown in Fig 10. We divide the dataset in the same proportions. Table 5 shows the data settings.

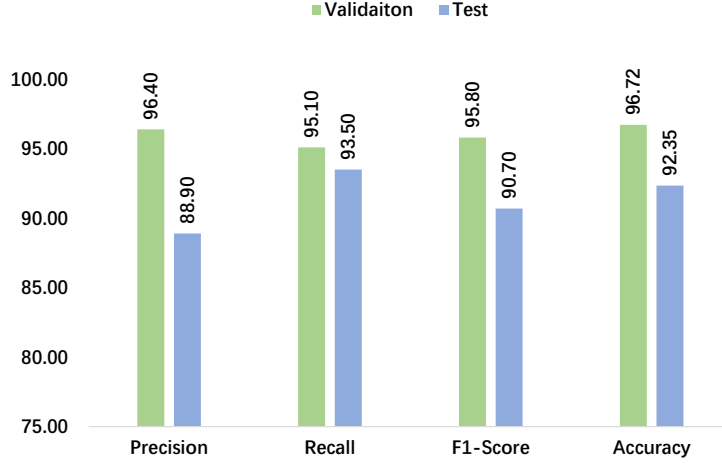


Figure 9: The performance of CVM-Cervix on Herlev dataset.

The performance of CVM-Cervix on the peripheral blood cell dataset is shown in Fig. 11. It can be seen that the precision, recall, F1-Score and accuracy on the validation set are 99.00%, 98.90%, 98.90% and 98.89%, respectively. The precision, recall, F1-Score and accuracy on the test set are 98.70%, 98.40%, 98.50% and 98.48%, respectively. CVM-Cervix performs very well on both the validation set and the test set of peripheral blood cell images and their difference is small. It indicates that CVM-Cervix performs well on other cell image datasets.

5. Discussion

5.1. Misclassification analysis and limitations of CVM-Cervix

To analyze the reasons for the misclassification, we use t-SNE method to map the 2240-dimensional feature vector into 3-dimensionality (3D) and visualize it [34]. Fig. 12 (a) shows the 3D scatter plot obtained using t-SNE. Some misclassified images and their feature maps are shown in Fig. 12 (b)-(f).

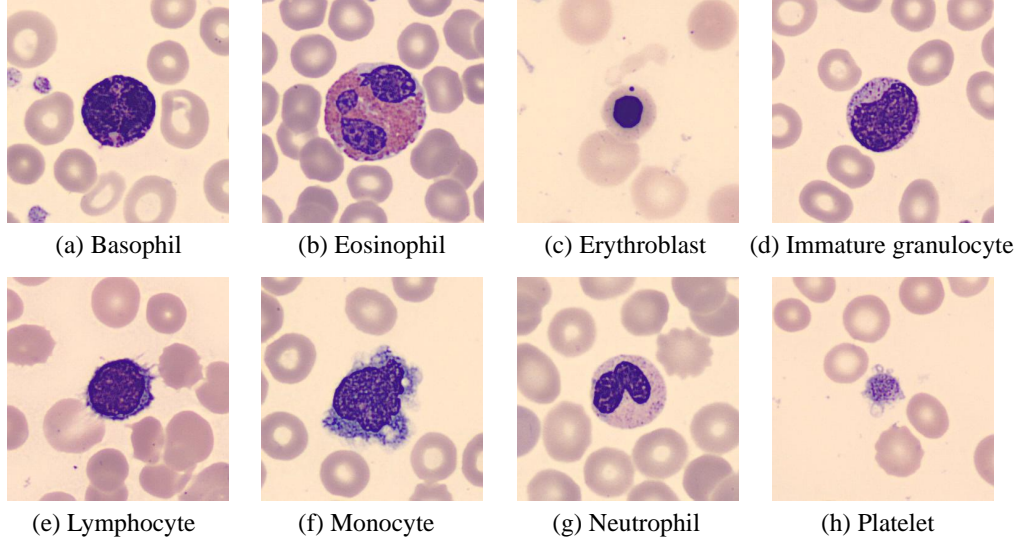


Figure 10: An example of images in peripheral blood cell dataset.

In Fig. 12 (b) and (c), ASC-US images are classified into LSIL and NILM. In Fig. 12 (e), the LSIL image is classified as ASC-US. In Fig. 12 (f), the LSIL image is classified as NILM. In medicine, these categories are adjacent. It can be seen that the nuclei of the four images are very similar and difficult to distinguish, which is also the main reason for the prediction error. From feature maps, we can see that features extracted by CVM-Cervix are inaccurate due to the light color of the cells and the unclear boundaries. In Fig. 12 (d), the Dyskeratotic image is classified as Koilocytotic. It can be seen that the background of the image is very dark, and the boundary between the nucleus and the cytoplasm is very blurred. The feature map also shows that CVM-Cervix cannot effectively identify cell nuclei when extracting the image features. In general, the similarity and ambiguity of images are the main reasons for classification errors.

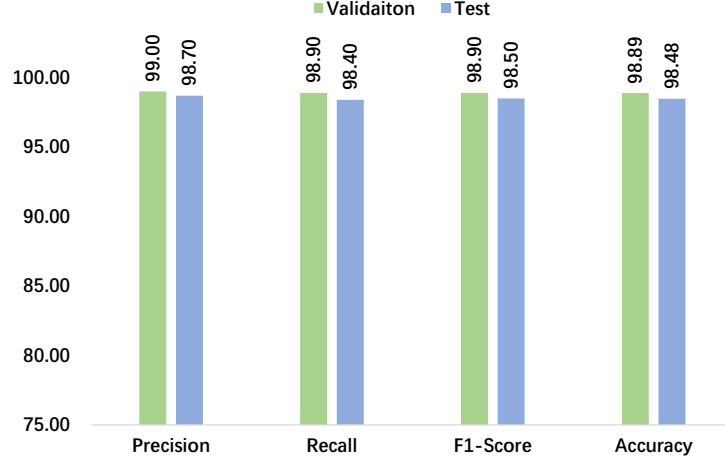


Figure 11: The performance of CVM-Cervix on peripheral blood cell dataset.

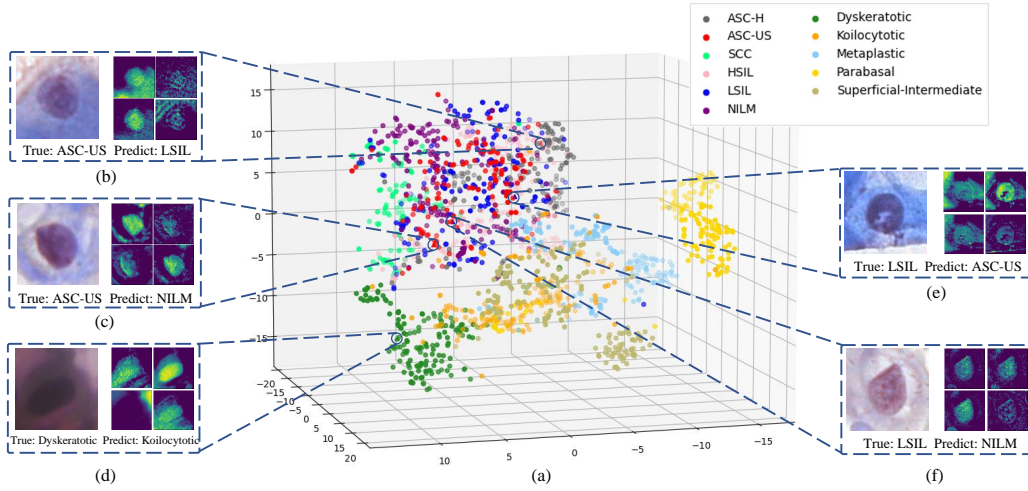


Figure 12: Visual analysis of misclassified images from the combined dataset. (a) is a 3D scatter plot obtained using t-SNE. (b)-(f) are misclassified images and their feature maps.

Table 5: Data settings of peripheral blood cell dataset.

Class/Dataset	Train	Validation	Test	Total
Basophil	731	244	243	1218
Eosinophil	1871	623	623	3117
Erythroblast	931	310	310	1551
Immature granulocyte	1737	579	579	2895
Lymphocyte	729	243	242	1214
Monocyte	852	284	284	1420
Neutrophil	1998	666	665	3329
Platelet	1409	470	469	2348
Total	10258	3419	3415	17092

Additionally, a limitation of our proposed CVM-Cervix method is that it is currently only performed on the classification task of cell images, and has not been experimented on other tasks.

5.2. Optimization strategy

Firstly, in the VT module of CVM-Cervix, we use a tiny DeiT model without distillation tokens. In the original paper of DeiT, the distillation module uses a teacher model to train a student model (ViT) [18]. In contrast, our CVM-Cervix integrates the DeiT module into the framework to use its global feature extraction capabilities and does not require a separate DeiT model. During pre-experiments, we use DeiT with the distillation module for experiments. However, we found that DeiT without the distillation module during fusion is more effective for our classification tasks.

Secondly, the optimizer and activation function should be chosen carefully. Although, there are various optimizers (e.g., Sobolev gradient based [35] and Lagrangian optimizer) and activation functions [36, 37] implemented with deep networks to solve different classification problems, we apply the AdamW and ReLU due to their efficiency in the proposed architecture with our datasets.

Finally, loss functions have an important role in a deep network architecture. To improve the performance of CNN-based architectures, hybrid loss functions have been proposed in several works [38]. We used the default loss function (i.e., cross-entropy) because of its low computational cost and efficiency with our images.

6. Conclusion and future work

This paper proposes a deep learning-based framework called CVM-Cervix for cervical cell classification tasks. CVM-Cervix first proposes a CNN module and a VT module for local and global feature extraction respectively, then a Multilayer Perceptron module is designed to fuse the local and global features for the final classification. CVM-Cervix is tested on a combined dataset of CRIC and SIPaKMeD datasets, and an accuracy of 91.72% is obtained for the 11-class classification problem. In addition, according to the practical needs of clinical work, we perform a lightweight post-processing to compress the model, where the model parameter size is compressed from 120 MB to 60 MB. In the extended experiment, CVM-Cervix is more efficient than the CNN and VT models alone. CVM-Cervix performs well on other cervical Pap smear and cell image datasets, indicating its strong generalization ability.

In the future, we will try to use more model combinations to improve CVM-Cervix performance. At the same time, the modification of the module structure can improve the feature extraction capability. Various data preprocessing techniques can be applied in the future to enhance the generalization capabilities of the model, such as color jittering and random cropping.

As another future work, the performance of the proposed approach will be compared with the performance of a capsule network since they can preserve spatial relationships of learned features and have been proposed recently for image classification [35, 39, 40].

Acknowledgements and Conflict of Interest

This work is supported by National Natural Science Foundation of China (No. 61806047). We thank Miss Zixian Li and Mr. Guoxian Li for their important discussion.

Conflict of Interest

The authors declare that they have no conflict of interest.

References

- [1] T. Šarenac, M. Mikov, Cervical cancer, different treatments and importance of bile acids as therapeutic agents in this disease, *Front. Pharmacol.* 10 (2019) 484.
- [2] A. Gençtav, S. Aksoy, S. Önder, Unsupervised segmentation and classification of cervical cell images, *Pattern Recognit.* 45 (12) (2012) 4151–4168.

- [3] E. Gocerı, C. Songul, Biomedical information technology: image based computer aided diagnosis systems, in: International Conference on Advanced Technologies, Antalya, Turkey, 2018.
- [4] Y. LeCun, Y. Bengio, G. Hinton, Deep learning, *nature* 521 (7553) (2015) 436–444.
- [5] E. Gocerı, Diagnosis of skin diseases in the era of deep learning and mobile technology, *Computers in Biology and Medicine* 134 (2021) 104458.
- [6] E. GÖÇERİ, An application for automated diagnosis of facial dermatological diseases, *İzmir Katip Çelebi Üniversitesi Sağlık Bilimleri Fakültesi Dergisi* 6 (3) (2021) 91–99.
- [7] E. Göçeri, Impact of deep learning and smartphone technologies in dermatology: Automated diagnosis, in: 2020 Tenth International Conference on Image Processing Theory, Tools and Applications (IPTA), IEEE, 2020, pp. 1–6.
- [8] A. Dosovitskiy, L. Beyer, A. Kolesnikov, D. Weissenborn, X. Zhai, T. Unterthiner, M. Dehghani, M. Minderer, G. Heigold, S. Gelly, et al., An image is worth 16x16 words: Transformers for image recognition at scale, *arXiv preprint arXiv:2010.11929* (2020).
- [9] M. E. Plissiti, P. Dimitrakopoulos, G. Sfıkas, C. Nikou, O. Krikoni, A. Charchanti, Sipakmed: A new dataset for feature and image based classification of normal and pathological cervical cells in pap smear images, in: 2018 25th IEEE International Conference on Image Processing (ICIP), IEEE, 2018, pp. 3144–3148.
- [10] M. T. Rezende, R. Silva, F. d. O. Bernardo, A. H. Tobias, P. H. Oliveira, T. M. Machado, C. S. Costa, F. N. Medeiros, D. M. Ushizima, C. M. Carneiro,

- et al., Cric searchable image database as a public platform for conventional pap smear cytology data, *Scientific Data* 8 (1) (2021) 1–8.
- [11] F. Chollet, Xception: Deep learning with depthwise separable convolutions, in: *2017 IEEE Conference on Computer Vision and Pattern Recognition (CVPR)*, 2017, pp. 1800–1807.
 - [12] K. Simonyan, A. Zisserman, Very deep convolutional networks for large-scale image recognition, *arXiv preprint arXiv:1409.1556* (2014).
 - [13] K. He, X. Zhang, S. Ren, J. Sun, Deep residual learning for image recognition, in: *Proceedings of the IEEE conference on computer vision and pattern recognition*, 2016, pp. 770–778.
 - [14] G. Huang, Z. Liu, L. Van Der Maaten, K. Q. Weinberger, Densely connected convolutional networks, in: *Proceedings of the IEEE conference on computer vision and pattern recognition*, 2017, pp. 4700–4708.
 - [15] Q. Wang, S. Liu, J. Chanussot, X. Li, Scene classification with recurrent attention of vhr remote sensing images, *IEEE Transactions on Geoscience and Remote Sensing* 57 (2) (2018) 1155–1167.
 - [16] Q. Wang, W. Huang, Z. Xiong, X. Li, Looking closer at the scene: Multiscale representation learning for remote sensing image scene classification, *IEEE Transactions on Neural Networks and Learning Systems* (2020).
 - [17] A. Srinivas, T.-Y. Lin, N. Parmar, J. Shlens, P. Abbeel, A. Vaswani, Bottleneck transformers for visual recognition, in: *2021 IEEE/CVF Conference on Computer Vision and Pattern Recognition (CVPR)*, 2021, pp. 16514–16524.

- [18] H. Touvron, M. Cord, M. Douze, F. Massa, A. Sablayrolles, H. Jegou, Training data-efficient image transformers & distillation through attention, in: Proceedings of the 38th International Conference on Machine Learning, Vol. 139, 2021, p. 1.
- [19] L. Yuan, Y. Chen, T. Wang, W. Yu, Y. Shi, F. E. Tay, J. Feng, S. Yan, Tokens-to-token vit: Training vision transformers from scratch on imagenet, arXiv preprint arXiv:2101.11986 (2021).
- [20] M. M. Rahaman, C. Li, X. Wu, Y. Yao, S. Qi, A survey for cervical cytopathology image analysis using deep learning, IEEE Access PP (99) (2020) 1–1.
- [21] H. Wieslander, G. Forslid, E. Bengtsson, C. Wahlby, J.-M. Hirsch, C. Runow Stark, S. Kecheril Sadanandan, Deep convolutional neural networks for detecting cellular changes due to malignancy, in: Proceedings of the IEEE International Conference on Computer Vision Workshops, 2017, pp. 82–89.
- [22] M. M. Rahaman, C. Li, Y. Yao, F. Kulwa, X. Wu, X. Li, Q. Wang, Deepcervix: A deep learning-based framework for the classification of cervical cells using hybrid deep feature fusion techniques, Comput. Biol. Med. 136 (2021) 104649.
- [23] J. Shi, R. Wang, Y. Zheng, Z. Jiang, H. Zhang, L. Yu, Cervical cell classification with graph convolutional network, Comput. Methods Programs Biomed. 198 (2021) 105807.
- [24] D. N Diniz, M. T Rezende, A. GC Bianchi, C. M Carneiro, E. JS Luz, G. JP Moreira, D. M Ushizima, F. NS de Medeiros, M. JF Souza, A deep

- learning ensemble method to assist cytopathologists in pap test image classification, *Journal of Imaging* 7 (7) (2021) 111.
- [25] T. Choudhary, V. Mishra, A. Goswami, J. Sarangapani, A comprehensive survey on model compression and acceleration, *Artificial Intelligence Review* 53 (7) (2020) 5113–5155.
 - [26] C. Szegedy, V. Vanhoucke, S. Ioffe, J. Shlens, Z. Wojna, Rethinking the inception architecture for computer vision, in: *Proceedings of the IEEE conference on computer vision and pattern recognition*, 2016, pp. 2818–2826.
 - [27] O. Russakovsky, J. Deng, H. Su, J. Krause, S. Satheesh, S. Ma, Z. Huang, A. Karpathy, A. Khosla, M. Bernstein, et al., Imagenet large scale visual recognition challenge, *Int. J. Comput. Vision* 115 (3) (2015) 211–252.
 - [28] C. Szegedy, W. Liu, Y. Jia, P. Sermanet, S. Reed, D. Anguelov, D. Erhan, V. Vanhoucke, A. Rabinovich, Going deeper with convolutions, in: *2015 IEEE Conference on Computer Vision and Pattern Recognition (CVPR)*, 2015, pp. 1–9.
 - [29] M. Sandler, A. Howard, M. Zhu, A. Zhmoginov, L.-C. Chen, Mobilenetv2: Inverted residuals and linear bottlenecks, in: *Proceedings of the IEEE conference on computer vision and pattern recognition*, 2018, pp. 4510–4520.
 - [30] N. Ma, X. Zhang, H.-T. Zheng, J. Sun, Shufflenet v2: Practical guidelines for efficient cnn architecture design, in: *Proceedings of the European conference on computer vision (ECCV)*, 2018, pp. 116–131.
 - [31] C. Szegedy, S. Ioffe, V. Vanhoucke, A. A. Alemi, Inception-v4, inception-resnet and the impact of residual connections on learning, in: *Proceed-*

- ings of the Thirty-First AAAI Conference on Artificial Intelligence, 2017, p. 4278–4284.
- [32] J. Jantzen, J. Norup, G. Dounias, B. Bjerregaard, Pap-smear benchmark data for pattern classification, *Nature inspired Smart Information Systems (NiSIS 2005)* (2005) 1–9.
 - [33] A. Acevedo, A. Merino, S. Alf  rez,   . Molina, L. Bold  , J. Rodellar, A dataset of microscopic peripheral blood cell images for development of automatic recognition systems, *Data in Brief*, ISSN: 23523409, Vol. 30,(2020) (2020).
 - [34] L. Van der Maaten, G. Hinton, Visualizing data using t-sne., *Journal of machine learning research* 9 (11) (2008).
 - [35] E. Goceri, Capsnet topology to classify tumours from brain images and comparative evaluation, *IET Image Processing* 14 (5) (2020) 882–889.
 - [36] E. Goceri, Skin disease diagnosis from photographs using deep learning, in: *ECCOMAS thematic conference on computational vision and medical image processing*, Springer, 2019, pp. 239–246.
 - [37] E. Goceri, Analysis of deep networks with residual blocks and different activation functions: classification of skin diseases, in: *2019 Ninth international conference on image processing theory, tools and applications (IPTA)*, IEEE, 2019, pp. 1–6.
 - [38] E. Goceri, Deep learning based classification of facial dermatological disorders, *Computers in Biology and Medicine* 128 (2021) 104118.

- [39] E. Goceri, Analysis of capsule networks for image classification, in: International Conference on Computer Graphics, Visualization, Computer Vision and Image Processing, 2021.
- [40] E. Goceri, Capsule neural networks in classification of skin lesions, in: International Conference on Computer Graphics, Visualization, Computer Vision and Image Processing, 2021.